Polymer Journal, Vol. 38, No. 1, pp. 64–72 (2006)

Wormlike Micelles of Pentaoxyethylene Tetradecyl Ether $C_{14}E_5$ and Hexaoxyethylene Hexadecyl Ether $C_{16}E_6$

Yoshiyuki EINAGA,† Yuko INABA, and Miwa SYAKADO

Department of Chemistry, Nara Women's University, Kitauoyanishi-machi, Nara 630-8506, Japan

(Received July 12, 2005; Accepted September 1, 2005; Published January 15, 2006)

ABSTRACT: Micelles of pentaoxyethylene tetradecyl $C_{14}E_5$ and hexaoxyethylene hexadecyl $C_{16}E_6$ ethers in dilute aqueous solutions were characterized by static (SLS) and dynamic light scattering (DLS) experiments at several temperatures T between the LCST and UCST phase boundaries. The SLS results were successfully analyzed with the aid of the thermodynamic theory formulated with wormlike spherocylinder model for SLS of micelle solutions, yielding the molar mass M_w of the micelles as a function of concentration c and the cross-sectional diameter d. The radius of gyration $\langle S^2\rangle^{1/2}$ of the micelles as a function of M_w was found to be well described by the corresponding theories for the wormlike chain model. Combining the present and previous results for various C_iE_j (polyoxyethylene alkyl ether) micelles, effects of the hydrophobic (alkyl) i and hydrophilic (oxyethylene) chain length j on the micellar characteristics have been clarified as: (i) The weight-average micellar length L_w becomes larger for larger i and smaller j. (ii) The d values do not significantly vary with the values of i and j. (iii) The stiffness parameter λ^{-1} decreases with increasing i at fixed j and increases with increasing j at fixed i. [DOI 10.1295/polymj.38.64]

KEY WORDS Polyoxyethylene Alkyl Ether / Micelle / Light Scattering / Radius of Gyration / Hydrodynamic Radius / Wormlike Spherocylinder /

In this series of experimental work on the wormlike micelles of polyoxyethylene alkyl ethers $H(CH_2)_i(OCH_2CH_2)_jOH$ (abbreviated C_iE_j),[1–6] we have investigated micellar characteristics by static (SLS) and dynamic light scattering (DLS) measurements and viscometry. We have determined the values of the molar mass $M_w(c)$ of the micelles at a specific c along with the cross-sectional diameter d from the analysis of the SLS data by using a molecular thermodynamic theory[7,8] formulated with the wormlike spherocylinder model. It is then found that molar mass M_w dependence of the mean-square radius of gyration $\langle S^2\rangle$, hydrodynamic radius R_H, and intrinsic viscosity $[\eta]$ is quantitatively represented by the chain statistical[9] and hydrodynamic[10–13] theories based on the wormlike chain and spherocylinder models, respectively, thereby yielding the values of the stiffness parameter λ^{-1} and/or d. These analyses have demonstrated that the C_iE_j micelles assume a shape of flexible cylinder. We have so far characterized micelles of the surfactants C_iE_j with various i and j, and examined effects of the hydrophobic i and hydrophilic chain length j on size, structure, and flexibility of the micelles. It has been shown that the C_iE_j micelles grow in size with raising temperature and increasing surfactant concentration, and that intermicellar thermodynamic and hydrodynamic interactions strongly increase with concentration.

The values of LCST (lower critical solution temperature) determined in our previous and present studies are summarized in Table I, in which the column and row represent variations in the length of the alkyl and oxyethylene chains of C_iE_j molecule, *i.e.*, i and j, respectively. The LCST decreases with increasing i at fixed j and with decreasing j at fixed i, reflecting that the micellar size varies with the hydrophobic and hydrophilic chain length i and j. The phase behavior may be in good correspondence with the observations for polymer solutions in which LCST decreases with increasing polymer molecular weight. Although the solution properties of micelles are analogous to those of polymer solutions, the micelles are essentially different from polymers in the point that the micellar size or length is not chemically fixed but, in general, depends on surfactant concentration. For this reason, analyses of the scattering data for micelle solutions encounter difficulties in the performance for separate determination of concentration-dependent micellar growth and intermicellar interactions. In order to circumvent this problem, we have utilized the molecular thermodynamic theory[7,8] for unequivocal determina-

Table I. Values of LCST/°C

	E_5	E_6	E_7	E_8
C_{10}	44.4	62.0		
C_{12}	32.0	51.7	65.5	
C_{14}	23.0	42.8	58.1	71.2
C_{16}		37.4	52.5	66.0
C_{18}			47.5	61.4

†To whom correspondence should be addressed (E-mail: einaga@cc.nara-wu.ac.jp).

tion of M_w of the micelles from the analysis of the SLS results in our previous studies.[1–5]

In the present study, we have extended our previous work[1–5] to the micelle solutions of the surfactants $C_{14}E_5$ and $C_{16}E_6$. The main aim is to examine the effects of the hydrophobic and hydrophilic chain lengths on the micellar characteristics such as length, cross-sectional diameter, and stiffness, in combination with the previous data for other C_iE_j micelles.

EXPERIMENTAL SECTION

Materials

The surfactant $C_{14}E_5$ and $C_{16}E_6$ samples were purchased from Nikko Chemicals Co. Ltd. and used without further purification. The solvent water used was high purity (ultrapure) water prepared with Simpli Lab water purification system of Millipore Co.

Phase Diagram

Cloud-point temperature of a given solution was determined as the temperature at which the intensity of the laser light transmitted through the solution abruptly decreased when temperature was gradually raised or lowered.

Static Light Scattering

SLS measurements were performed to obtain the weight-average molar mass M_w of the $C_{14}E_5$ and $C_{16}E_6$ micelles. The scattering intensities were measured for each solution and for the solvent water at scattering angles θ ranging from 30 to 150° and at several temperatures T ranging from 10.0 to 20.0 °C for $C_{14}E_5$ solutions and from 24.0 to 35.0 °C for $C_{16}E_6$ solutions. The ratio $Kc/\Delta R_\theta$ was obtained for each solution as a function of θ and extrapolated to zero scattering angle to evaluate $Kc/\Delta R_0$. Here, c is the surfactant mass concentration, ΔR_θ is the excess Rayleigh ratio, and K is the optical constant defined as

$$K = \frac{4\pi^2 n^2 (\partial n/\partial c)_{T,p}^2}{N_A \lambda_0^4} \tag{1}$$

with N_A being the Avogadro's number, λ_0 the wavelength of the incident light in vacuum, n the refractive index of the solution, $(\partial n/\partial c)_{T,p}$ the refractive index increment, T the absolute temperature, and p the pressure. The plot of $Kc/\Delta R_\theta$ *vs.* $\sin^2(\theta/2)$ affords a good straight line for all the micelle solutions studied. From the slope of the straight line, we have determined the apparent mean-square radius of gyration $\langle S^2 \rangle_{app}$ for the micelles at finite concentrations on the basis of the fundamental light scattering equation

$$\frac{Kc}{\Delta R_\theta} = \frac{1}{M_w(c)} \left(1 + \frac{1}{3} \langle S^2 \rangle q^2 \right) + 2A_2 c + \cdots \tag{2}$$

by using the $M_w(c)$ values determined as described below. Here, A_2 is the second virial coefficient and q is the magnitude of the scattering vector defined as

$$q = \frac{4\pi n}{\lambda_0} \sin(\theta/2) \tag{3}$$

The mean square radius of gyration $\langle S^2 \rangle$ is denoted by $\langle S^2 \rangle_{app}$, since it is possibly affected by intermicellar interactions at finite concentrations examined.

The apparatus used is an ALV DLS/SLS-5000/E light scattering photogoniometer and correlator system with vertically polarized incident light of 632.8 nm wavelength from a Uniphase Model 1145P He–Ne gas laser. For a calibration of the apparatus, the intensity of light scattered from pure benzene was measured at 25.0 °C at a scattering angle of 90°, where the Rayleigh ratio $R_{UV}(90)$ of pure benzene for unpolarized scattered light with polarized incident light at a wavelength of 632.8 nm was taken as 11.84×10^{-6} cm^{-1}.[14,15]

The micellar solutions were prepared by dissolving appropriate amount of the surfactant in water. Complete mixing and micelle formation were achieved by stirring using a magnetic stirrer at least for one day. The solutions thus prepared were optically clarified by filtration through a membrane of 0.20 μm pore size and transferred into optically clean NMR tubes of 10 mm diameter which was used as scatterring cells. The weight concentrations w of test solutions were determined gravimetrically and converted to mass concentrations c by the use of the densities ρ of the solutions given below.

The refractive index increment $(\partial n/\partial c)_{T,p}$ was measured at 10.0, 15.0, and 20.0 °C for $C_{14}E_5$ solutions and at 25.0, 30.0, and 35.0 °C for $C_{16}E_6$ solutions at 632.8 nm with a Union Giken R601 differential refractometer. The results were found to be independent of T and 0.1321 cm^3/g for the former and 0.1312 cm^3/g for the latter.

Dynamic Light Scattering

DLS measurements were carried out to determine the translational diffusion coefficient D and then hydrodynamic radius R_H of the micelles at several temperatures in the one phase (L_1 phase) region between the phase separation boundaries shown below by the use of the same apparatus and light source as used in the SLS studies described above. The normalized autocorrelation function $g^{(2)}(t)$ of scattered light intensity $I(t)$, *i.e.*,

$$g^{(2)}(t) = \frac{\langle I(0)I(t) \rangle}{\langle I(0) \rangle^2} \tag{4}$$

was measured at scattering angles θ ranging from 30 to 150°.

All the test solutions studied are the same as those used in the SLS studies. From the data for $g^{(2)}(t)$, we determined D by the equation

$$(1/2)\ln[g^{(2)}(t) - 1] = (1/2)\ln f - K_1 t + \cdots \quad (5)$$

$$D = \lim_{q \to 0} K_1/q^2 \quad (6)$$

Here, f is the coherence factor fixed by the optical system and K_1 is the first cumulant. It should be noted that the D values should be regarded as an average, since the micelles observed may have distribution in size.

The apparent hydrodynamic radius $R_{H,app}$ has been evaluated from the D values by[1,16,17]

$$D = \frac{(1 - vc)^2 M_w k_B T}{6\pi\eta_0 R_{H,app}} \left(\frac{Kc}{\Delta R_0}\right) \quad (7)$$

where v is the partial specific volume of the solute (micelle), k_B is the Boltzmann constant, and η_0 is the solvent viscosity.

Density

The solution density ρ required for the calculation of c and v was measured at 10.0, 15.0 and 20.0 °C for $C_{14}E_5$ solutions and at 25.0, 30.0, and 35.0 °C for $C_{16}E_6$ solutions with a pycnometer of the Lipkin–Davison type. For the two micelle solutions, ρ has been found to be independent of surfactant weight fraction w at every temperature examined. We have, thus, used the literature values of the density ρ_0 of pure water at corresponding temperatures for ρ, and the values of v of the micelles have been calculated as ρ_0^{-1}.

RESULTS

Phase Behavior

In Figure 1 are depicted the cloud point curves for the aqueous solutions of $C_{14}E_5$ (unfilled circles) and $C_{16}E_6$ (filled circles). It is seen that both the micelle solutions represent the phase separation behavior of the LCST and UCST (upper critical solution temperature) type and then the L_1 phase (uniform micelle solution phase) is limitted to narrow temperature range in between the two phase boundaries.

Light Scattering Results

In Figure 2, $Kc/\Delta R_0$ are plotted against c for all the solutions of the $C_{14}E_5$ and $C_{16}E_6$ micelles at various temperatures indicated. The data points at fixed T follow a curve convex downward and the $Kc/\Delta R_0$ value at fixed c decreases with increasing T.

Figure 3 illustrates the plots of D against c determined from the $g^{(2)}(t)$ data by the cumulant method with eqs 5 and 6 for the $C_{14}E_5$ and $C_{16}E_6$ micelles at various temperatures indicated. The D value becomes smaller as T is raised, for any case of the micelle solutions. It is seen that D for the $C_{14}E_5$ micelles increases rather steeply with increasing c at c higher than *ca.* 0.005 g/cm^3, while that for the $C_{16}E_6$ micelles decreases rather sharply at small c and then gradually increases as c is increased.

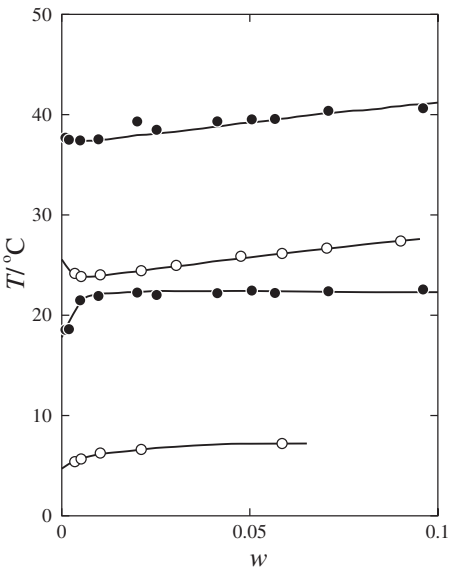

Figure 1. Cloud point curves for the $C_{14}E_5$ (unfilled circles) and $C_{16}E_6$ (filled circles) micelle solutions.

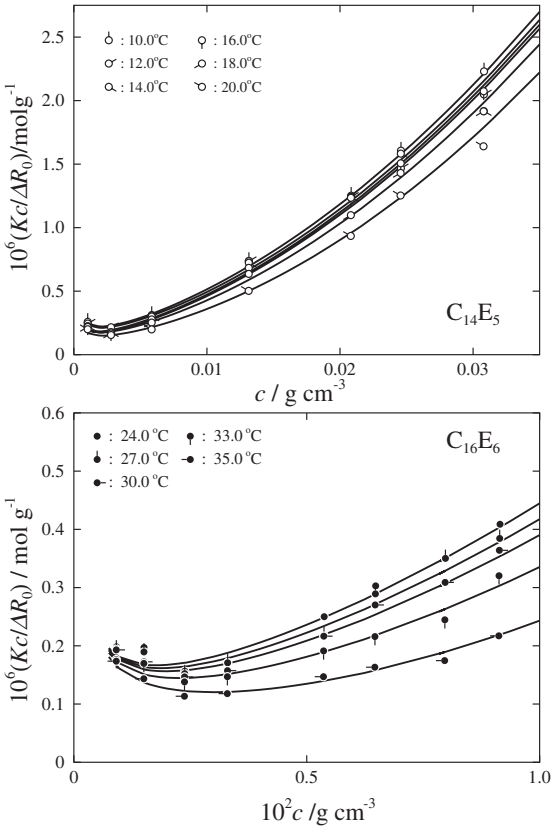

Figure 2. Concentration dependence of $Kc/\Delta R_0$ for the $C_{14}E_5$ and $C_{16}E_6$ micelle solutions at various temperatures indicated.

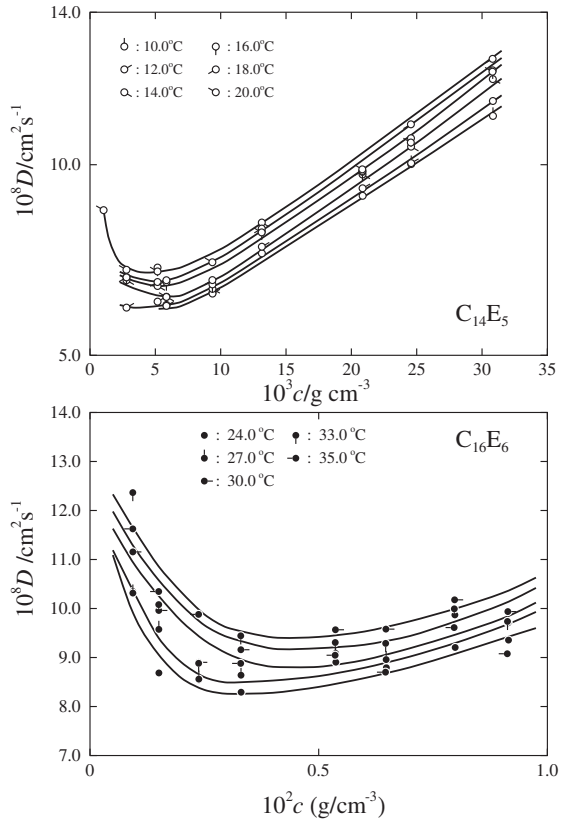

Figure 3. Concentration dependence of the diffusion coefficient D for the $C_{14}E_5$ and $C_{16}E_6$ micelles at various temperatures indicated.

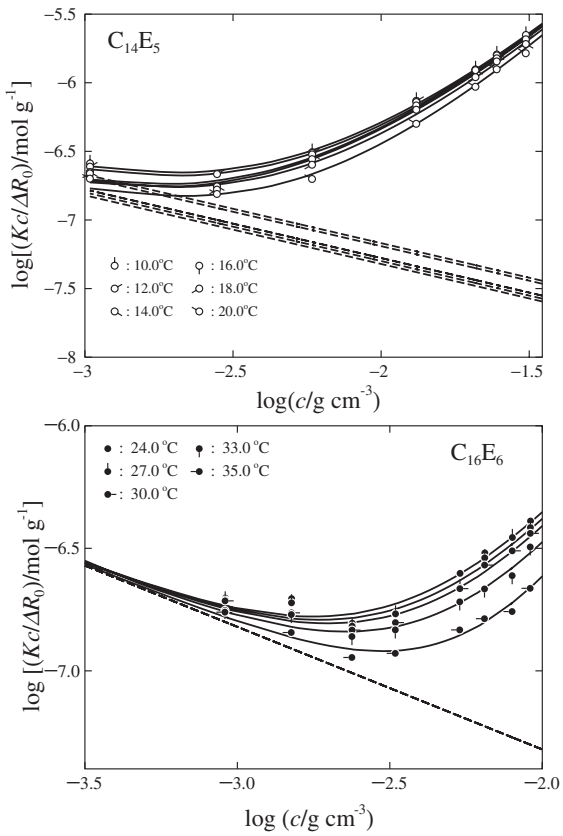

Figure 4. Results for the curve fitting for the bilogarithmic plots of $Kc/\Delta R_0$ *vs.* c for the $C_{14}E_5$ and $C_{16}E_6$ micelle solutions at various temperatures indicated. The solid and dashed lines represent the theoretical values of $Kc/\Delta R_0$ and $1/M_w$, respectively.

DISCUSSION

Analysis of SLS Data

In order to determine the M_w values of the micelles at a specific concentration c, we have analyzed the SLS data by employing a light-scattering theory for micellar solutions formulated by Sato[7,8] with wormlike spherocylinder model as mentioned in the Introduction. The model consists of a wormlike cylinder of contour length $L - d$ with cross-sectional diameter d and two hemispheres of diameter d which cap both ends of the cylinder, and stiffness of the wormlike cylinder is represented by the stiffness parameter λ^{-1}. It may represent a variety of the shape of polymer-like micelles, including a sphere, rigid rod, flexible and/or random-coil rod (or cylinder). The result for $Kc/\Delta R_0$ reads

$$\frac{Kc}{\Delta R_0} = \frac{1}{M_w(c)} + 2A(c)c \tag{8}$$

where $M_w(c)$ is the weight-average molar mass of the micelles and $A(c)$ is the apparent second virial coefficient in a sense that it is comprised of the second, third, and the higher virial coefficient terms. Both are functions of c, containing three parameters d, free-energy parameter g_2, and strength $\hat{\varepsilon}$ of the attractive interaction between spherocylinders. In these, g_2 represents the difference in Gibbs free energy between surfactant molecules located in the end-capped portion to those in the central cylindrical portion in the micelle. The parameter $\hat{\varepsilon}$ is the depth of the attractive potential between cylindrical micelles. It should be noted that the aggregation number N is essentially governed by multiple equilibria among the micelles with various N and by the intermicellar interactions to some extent.[18] The parameters g_2 and $\hat{\varepsilon}$ play dominant role in the former and in the latter, respectively. We refer the expressions for the functions $M_w(c)$ and $A(c)$ to the original papers (ref 7 and 8) and our previous papers,[1,3] since they are fairly involved.

Figure 4 demonstrates the results of curve-fitting of the theoretical calculations to the experimental values of $Kc/\Delta R_0$ for the $C_{14}E_5$ and $C_{16}E_6$ micelle solutions. In the performance, we have calculated the theoretical values of $Kc/\Delta R_0$ as a function of c for various sets of the values of d, g_2, and $\hat{\varepsilon}$, and chosen the best-fit one to the observed results at each fixed T for respective micelle solutions. The curve fittings have yielded the $M_w(c)$ values of the micelles at finite concentrations at each T. The solid curves in the figures represent the best-fit theoretical curves thus determined. It is seen

that they are in good coincidence with the respective data points at given temperatures, implying that the $C_{14}E_5$ and $C_{16}E_6$ micelles in dilute aqueous solutions are represented by the wormlike spherocylinder model. The dashed lines represent the values of $1/M_w(c)$ at respective temperatures. The data points for all the micelles at any fixed T follow a straight line with a slope of -0.5. The results show that M_w increases with c as $M_w \propto c^{1/2}$ in the range of c examined, as in the case of the previous findings for the $C_{12}E_6$ and $C_{14}E_6$ micelles,[1] for the $C_{14}E_8$, $C_{16}E_8$ and $C_{18}E_8$ micelles,[2] for the $C_{10}E_5$ and $C_{12}E_5$ micelles,[3] for the $C_{16}E_7$ and $C_{18}E_7$ micelles,[4] and for the $C_{12}E_5$, $C_{12}E_7$, and $C_{14}E_7$ micelles.[5] These results are in good correspondence with simple theoretical predictions derived from the thermodynamic treatments of multiple equilibria among micelles of various aggregation numbers.[7,18–20] It is to be noted that the the M_w *vs.* c relations for the $C_{16}E_6$ micelles are independent of T. The solid and dashed curves tend to coincide with each other at small c and the difference between them steadily increases with increasing c. The results indicate that contributions of the virial coefficient terms, that is, the second term of the right hand side of eq 8, to $Kc/\Delta R_0$ become negligible at small c but progressively increase with increasing c as expected.

The d value obtained for both the $C_{14}E_5$ and $C_{16}E_6$ micelles is 2.5 nm at any T examined. The values of g_2 and $\hat{\varepsilon}$ determined are plotted against T in Figure 5. For each micelle, $\hat{\varepsilon}$ increases with raising temperature, while g_2 does not show clear systematic dependence on T. It may be underscored that g_2 for the $C_{16}E_6$ micelles are independent of T corresponding to the finding that M_w of the micelles does not depend on T.

Molar Mass Dependence of Radius of Gyration

The values of $\langle S^2\rangle_{app}^{1/2}$ determined at various T and c

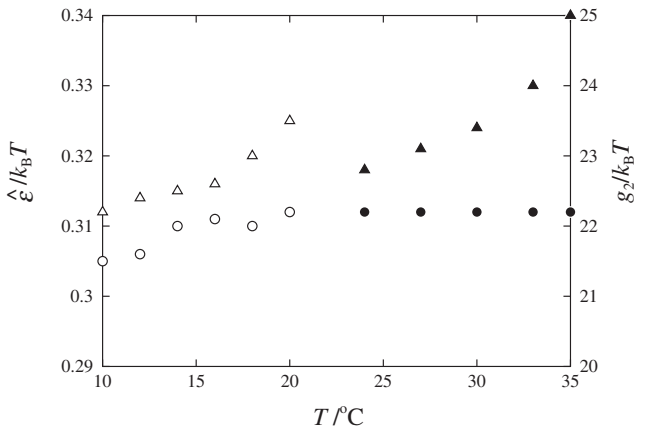

Figure 5. Temperature dependence of $\hat{\varepsilon}$ (triangles) and g_2 (circles) for the $C_{14}E_5$ (unfilled symbols) and $C_{16}E_6$ (filled symbols) micelle solutions.

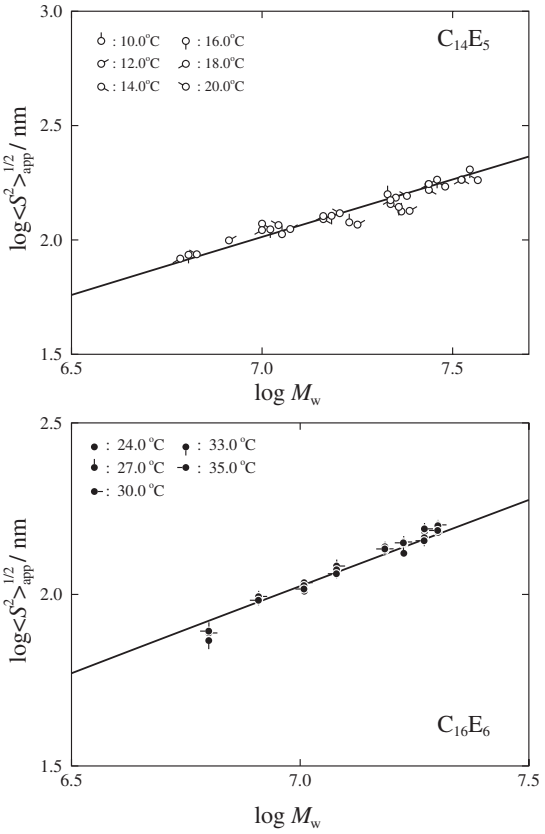

Figure 6. Bilogarithmic plots of $\langle S^2\rangle_{app}^{1/2}$ against M_w for the $C_{14}E_5$ and $C_{16}E_6$ micelles at various temperatures indicated. The solid curves represent the theoretical values calculated by eqs 9 and 10.

by eq 2 for the $C_{14}E_5$ and $C_{16}E_6$ micelles are bilogarithmically plotted against M_w in Figure 6. For each of the micelles, the data points at various T and c are found to form a single composite curve, suggesting that the values of $\langle S^2\rangle_{app}^{1/2}$ determined at finite c correspond to those of $\langle S^2\rangle^{1/2}$ for the individual micelles free from inter- and intra-micellar interactions or excluded volume effects. Thus, we have analyzed them by using the equation for the wormlike chain model written as[9]

$$\lambda^2\langle S^2\rangle = \frac{\lambda L}{6} - \frac{1}{4} + \frac{1}{4\lambda L} - \frac{1}{8\lambda^2 L^2}(1 - e^{-2\lambda L}) \quad (9)$$

along with the relation

$$L_w = \frac{4\nu M_w}{\pi N_A d^2} + \frac{d}{3} \quad (10)$$

Here, the relation between L_w and M_w is derived from the micellar volume and L_w is used in place of L in eq 9.

The solid curves in Figure 6 show the best-fit theoretical values of $\langle S^2\rangle^{1/2}$ for each micelle. Here, we have used the values of d determined above from the analyses of the SLS data and then evaluated λ^{-1} as 19.0 and 20.0 nm for the $C_{14}E_5$ and $C_{16}E_6$ micelles,

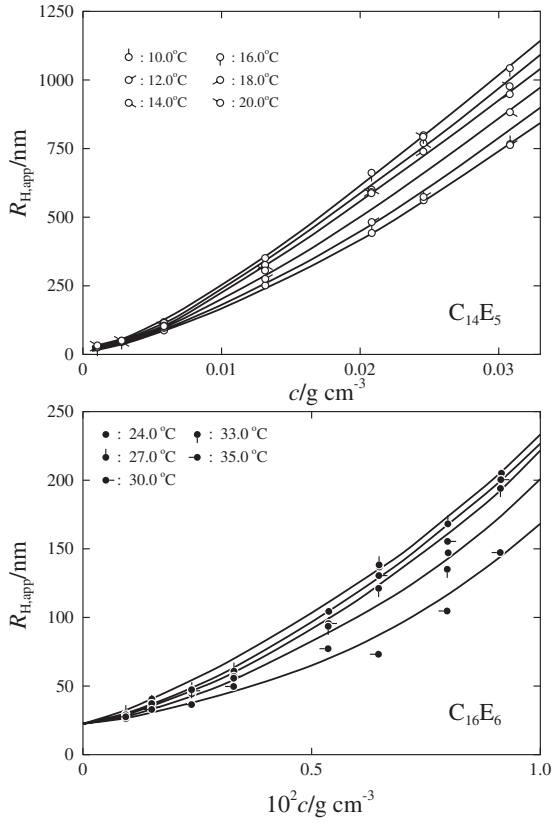

Figure 7. Concentration dependence of R_H for the $C_{14}E_5$ and $C_{16}E_6$ micelles at various temperatures indicated.

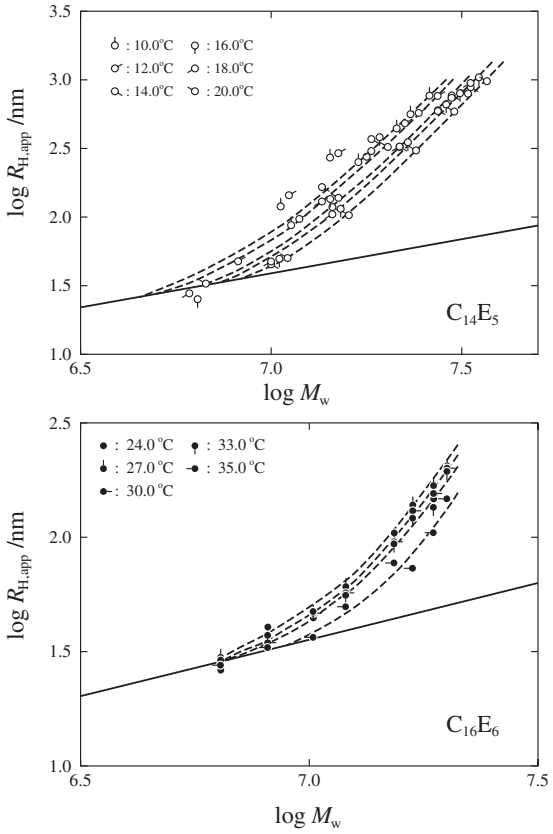

Figure 8. Bilogarithmic plots of R_H against M_w for the $C_{14}E_5$ and $C_{16}E_6$ micelles at various temperatures indicated. The solid curves represent the theoretical values calculated by eqs 10 and 11.

respectively. It is found that the calculated results well explains the observed behavior of $\langle S^2\rangle_{app}^{1/2}$. This agreement again shows that the $C_{14}E_5$ and $C_{16}E_6$ micelles assume a shape of wormlike spherocylinder.

Hydrodynamic Radius of the Micelles

The values of $R_{H,app}$ determined by eq 7 for $C_{14}E_5$ and $C_{16}E_6$ micelles at various T and c are plotted against c in Figure 7. It is found that the values of $R_{H,app}$ at fixed c are larger for higher T and $R_{H,app}$ at any given T increases with increasing c. The increase of $R_{H,app}$ does not necessarily correspond to the micellar growth with increasing T and c. The concentration dependence of $R_{H,app}$ reflects two effects; micellar growth in size and enhancement of the effects of the intermicellar hydrodynamic interactions with increasing c.

Figure 8 shows bilogarithmic plots of $R_{H,app}$ against M_w for the $C_{14}E_5$ and $C_{16}E_6$ micelles. As M_w is decreased, *i.e.*, c is lowered, $R_{H,app}$ at fixed T decreases following the curve convex downward shown by the dashed line. These results implies that the effects of the intermicellar hydrodynamic interactions on $R_{H,app}$ become less significant as c is lowered. In our previous papers,[1–3] it has been indicated that in similar plots, the data points at different T asymptotically form a single composite curve at low c, or small M_w, providing the relationship between R_H and M_w for "isolated" micelles. According to the previous findings, we have analyzed the data points at small M_w at each fixed T in Figure 8 by the hydrodynamic theories given by Norisuye *et al.*[10] for the wormlike spherocylinder model and by Yamakawa *et al.*[11,12] for the wormlike cylinder model, although the data points are rather scarce. The equation for R_H reads

$$R_H = \frac{L}{2f(\lambda L, \lambda d)} \tag{11}$$

The expression for the function f is so lengthy that we refer it to the original papers.[10–12] By eqs 10 and 11, the theoretical values of R_H have been calculated as a function of M_w for various values of λ^{-1} with the use of the d value 2.5 nm determined above for the $C_{14}E_5$ and $C_{16}E_6$ micelles. Here, L in eq 11 is replaced by L_w given by eq 10. In Figure 8, the solid lines represent best-fit curves to the data points for which the effects of the intermicellar hydrodynamic interactions are considered to be negligible. The data points at fixed T steeply increase with M_w deviating upward from the solid curve due to the enhancement of the intermicellar hydrodynamic interactions with increasing c.

From the curve fittings, we have obtained 6.0 and

5.0 nm for the λ^{-1} values of the $C_{14}E_5$ and $C_{16}E_6$ micelles, respectively. The λ^{-1} values are significantly smaller than those obtained above from the analyses of $\langle S^2 \rangle$. This difference may be attributed to the fact that there is a distribution in micellar size and different averages are reflected in $\langle S^2 \rangle_{app}^{1/2}$ and R_H. Sato[7] and Zoeller *et al.*[18] have theoretically shown that micelles with sufficiently large aggregation number N have the most probable distribution and the distribution affords a value *ca.* 2 as the ratio of the weight-average aggregation number N_w to the number-average N_n without regard to the existence of the inter- and intra-micellar thermodynamic or excluded-volume interactions. They have also showed that in the limit of extensive micellar growth, the relation $M_w \propto c^{1/2}$ is set up, as observed in Figure 4 in the present case. It is, thus, anticipated that the micelles observed in this study are grown up to the degree long enough to realize the most probable distribution in size and the distribution affects the evaluation of λ^{-1} from $\langle S^2 \rangle^{1/2}$ and R_H. Sato[7] has discussed the effects of the micelle size distribution on $\langle S^2 \rangle$ in his theory. The theoretical results for the effects on R_H are not, however, available at present. Thus, we leave the evaluation of the effects of the micellar size distribution on λ^{-1} for future work.

Length of the Micelles

The weight-average micellar length L_w was calculated by eq 10 from the values of $M_w(c)$ and d obtained above from the analyses of the SLS data. The results for the $C_{14}E_5$ micelles at 20.0 °C and the $C_{16}E_6$ at 30.0 °C are plotted against c in Figure 9. It is seen that the data points for the two micelles accidentally follow the same straight line with a slope 0.5. The results are in correspondence to the fact that M_w increases with c following a relation $M_w \propto c^{1/2}$ as shown in Figure 4.

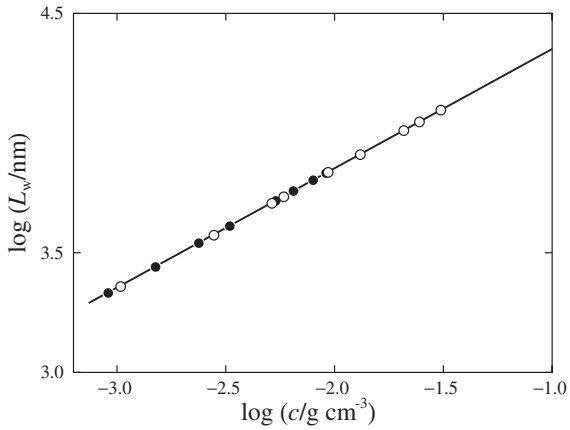

Figure 9. Bilogarithmic plots of L_w against c for the $C_{14}E_5$ micelles at 20.0 °C (unfilled circles) and $C_{16}E_6$ micelles at 30.0 °C (filled circles).

The L_w values of the $C_{14}E_5$ micelles at three concentrations are plotted against T in Figure 10, in which those for the other C_iE_j micelles are also included. It is found that the C_iE_5 micelles grow to a greater length as longer the alkyl chain length i of the surfactant molecules. In this case, the number of the oxyethylene units in the hydrophilic group is fixed to 5 and then the strength in the repulsive force between the adjacent oxyethylene chains may remain constant for different C_iE_5 micelles. On the other hand, attractive force among alkyl chains of the surfactant molecules due to the hydrophobic interactions is considered to become stronger as i is increased. The effects may facilitate the growth of micelles to the greater length for the surfactant C_iE_5 with longer alkyl chain.

As seen in Figure 10, the length L_w of the micelles

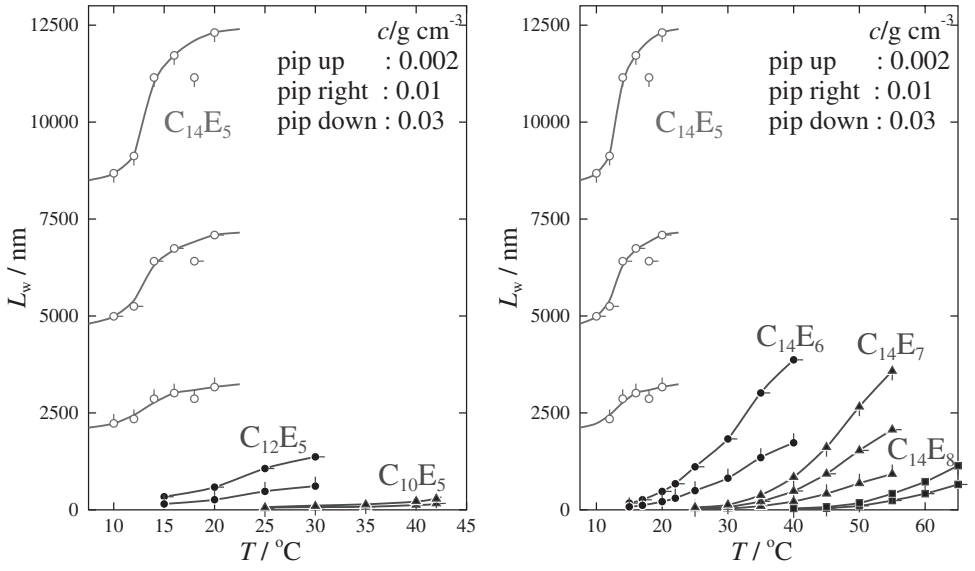

Figure 10. Temperature dependence of L_w for various C_iE_j micelles at indicated concentrations.

$C_{14}E_j$ becomes shorter with increasing oxyethylene chain length j. This finding may be interpreted as follows. Since water is a good solvent for polyoxyethylene, the oxyethylene group of the surfactant C_iE_j molecule opt to join the surrounding water molecules, which stabilizes the micelle in water. The affinity among the oxyethylene groups and water molecules causes repulsive force between the adjacent oxyethylene chains on the surface of the micelle, for the one end of the chain is fixed to the micelle core. The repulsive force is considered to be stronger for longer the oxyethylene group and it works to make more surface area of the micelle. This may be the reason why the $C_{14}E_j$ molecules form shorter micelles with increasing j.

The Cross-sectional Diameter d and Stiffness Parameter λ^{-1} of the Micelles

The values of d and λ^{-1} obtained for the C_iE_j micelles in the present and previous studies[1–5] are summarized in Tables II and III, respectively, Here, d and λ^{-1} are evaluated from the analyses of the SLS results and R_H as a function of M_w, respectively. Here, we note that the λ^{-1} value has not been obtaned from $\langle S^2 \rangle$ for all the C_iE_j micelles, since some of the micelles are not long enough to determine $\langle S^2 \rangle$ with sufficient accuracy. In the Tables, the column and row represent the alkyl and oxyethylene chain lengths, respectively.

We find in Table II that the d value does not significantly vary with hydrophobic and hydrophilic chain length. The results imply that the alkyl and oxyethylene groups of C_iE_j molecules do not take a fully extended or *trans* zig-zag form but assume a randomly coiled form in the micelles, as mentioned in the previous papers.[1–3,5] Table III shows that λ^{-1} decreases with increasing alkyl chain length i at fixed j except for the C_iE_8 micelles and increases with j at fixed i.

Table II. Values of the Cross-Sectional Diameter d/nm

	E_5	E_6	E_7	E_8
C_{10}	2.6	2.6		
C_{12}	2.2	2.3	2.4	
C_{14}	2.5	2.4	2.4	2.3
C_{16}		2.5	2.5	2.4
C_{18}			2.5	3.2

Table III. Values of the Stiffness Parameter λ^{-1}/nm

	E_5	E_6	E_7	E_8
C_{10}	35.0	75.0		
C_{12}	12.0	14.0	14.0	
C_{14}	6.0	7.0	13.0	18.0
C_{16}		5.0	6.0	24.0
C_{18}			6.0	25.0

This suggests that the relative strength of the repulsive force due to the hydrophilic interaction among C_iE_j molecules in the micelle to the attractive force due to the hydrophobic interactions controls the stiffness parameter; the repulsive force between the adjacent oxyethylene chains contribute to make the micelles stiffer and the attractive force between the adjacent alkyl chains reduce stiffness.

CONCLUSIONS

In the present work, we have studied the $C_{14}E_5$ and $C_{16}E_6$ micelles by static (SLS) and dynamic light scattering (DLS) experiments by employing the same technique as used in the previous studies.[1–5] The results of $Kc/\Delta R_0$ from SLS have been analyzed with the aid of the thermodynamic theory[7] for light scattering of micelle solutions formulated with wormlike spherocylinder model. The procedure has yielded the molar mass $M_w(c)$ as a function of c along with the cross-sectional diameter d of the micelle. The good agreement between the calculated and observed $Kc/\Delta R_0$ as a function of c indicates that the micelles examined assume a shape of flexible spherocylinders in dilute solutions. It is also found that the mean-square radius of gyration $\langle S^2 \rangle$ of the individual "isolated" micelles as a function of M_w have been well described by the theory for the wormlike chain model.

From the analyses of the SLS and DLS results, we have evaluated micellar length L_w as a function of surfactant concentration c and temperature T, d, and the stiffness parameter λ^{-1}. Combining the present and previous[1–5] results for these quantities, we have examined effects of the hydrophobic (alkyl) i and hydrophilic (oxyethylene) chain length j on the characteristics of C_iE_j micelles. Salient features found are summarized as follows: (i) The micelles grow in length to a greater extent for larger i and smaller j, reflecting that among surfactant molecules, attractive force due to the hydrophobic interactions becomes stronger for larger i and repulsive force due to the hydrophilic interactions becomes stronger for larger j. (ii) The d values do not significantly vary with the values of i and j, indicating that the alkyl and oxyethylene chains of the surfactant molecule assume a random-coil form. (iii) The stiffness parameter λ^{-1} decreases with increasing i at fixed j and increases with increasing j at fixed i, suggesting that the stiffness of the micelle is controlled by the relative strength of the repulsive force to the attractive one among the surfactant molecules.

Acknowledgment. This research was supported in part by Nara Women's University Intramural Grant for Project Research.

REFERENCES

1. S. Yoshimura, S. Shirai, and Y. Einaga, *J. Phys. Chem. B.*, **108**, 15477 (2004).
2. N. Hamada and Y. Einaga, *J. Phys. Chem. B.*, **109**, 6990 (2005).
3. K. Imanishi and Y. Einaga, *J. Phys. Chem. B.*, **109**, 7574 (2005).
4. Y. Einaga, A. Kusumoto, and A. Noda, *Polym. J.*, **37**, 368 (2005).
5. S. Shirai and Y. Einaga, *Polym. J.*, in press.
6. S. Shirai, S. Yoshimura, and Y. Einaga, *Polym. J.*, in press.
7. T. Sato, *Langmuir*, **20**, 1095 (2004).
8. R. Koyama and T. Sato, *Macromolecules*, **35**, 2235 (2002).
9. H. Benoit and P. Doty, *J. Phys. Chem.*, **57**, 958 (1953).
10. T. Norisuye, M. Motowoka, and H. Fujita, *Macromolecules*, **12**, 320 (1979).
11. H. Yamakawa and M. Fujii, *Macromolecules*, **6**, 407 (1973).
12. H. Yamakawa and T. Yoshizaki, *Macromolecules*, **12**, 32 (1979).
13. T. Yoshizaki, I. Nitta, and H. Yamakawa, *Macromolecules*, **21**, 165 (1988).
14. E. R. Pike, R. M. Pomeroy, and J. M. Vaughan, *J. Chem. Phys.*, **62**, 3188 (1975).
15. Y. Einaga, T. Mitani, J. Hashizume, and H. Fujita, *Polym. J.*, **11**, 565 (1979).
16. B. Berne and R. Pecora, "Dynamic Light Scattering," J. Wiley, New York, 1976.
17. P. Štěpánek, W. Brown, and S. Hvidt, *Macromolecules*, **29**, 8888 (1996).
18. N. Zoeller, L. Lue, and D. Blankschtein, *Langmuir*, **13**, 5258 (1997).
19. D. Blankschtein, G. M. Thurston, and G. B. Benedek, *J. Chem. Phys.*, **85**, 7268 (1986).
20. M. E. Cates and S. J. Candou, *J. Phys.: Condens. Matter*, **2**, 6869 (1990).